Interfaces in as-extruded XD Al/TiC and Al/TiB$_2$ metal matrix composites

R. Mitra, W. A. Chiou, M. E. Fine, and J. R. Weertman
*Department of Materials Science and Engineering, Northwestern University,
Evanston, Illinois 60208-3108*

A detailed study was conducted of the microstructure and particle-matrix interfaces in Al/TiC$_p$ metal matrix composites prepared by the XD process and subsequent extrusion. A study of the morphology of the TiC particles showed that the surfaces are low index (111) and (200) planes, the former being more common. Direct contact on an atomic scale is established between Al and TiC, allowing chemical bonds to form. Young's modulus is in the range expected for a composite of Al and TiC with good interfacial bonding and load transfer to the particles. No third element has been detected at the interfaces, showing that they are clean. Both incoherent and semicoherent interfaces are seen. The interface character depends on the size of the particles and their orientation with respect to the neighboring Al grains. "Special" interfaces with evidence for nearly periodic dislocations were observed in both XD Al/TiC and Al/TiB$_2$ composites, indicating the general tendency of *in situ* composites to lower their interfacial energy by forming such boundaries.

I. INTRODUCTION

Aluminum-based metal matrix composites are designed to combine the ductility of the Al matrix and the strength and modulus of the reinforcement phase. Considerable improvement can be obtained in the strength, stiffness, and wear resistance of composites compared to those properties in monolithic metals and alloys. However, often it is seen that the gains in the above properties fall short of theoretical expectations and the ductility is limited. Behavior may vary in the same composite system depending on the processing method. Load transfer from the matrix to the hard ceramic reinforcement, dislocation-particle interactions, and fracture depend on the properties of the interface region. Both efficiency of load transfer at a metal-ceramic interface and plastic deformation in the vicinity depend to a large extent on whether the bonding is mechanical or chemical. If chemical, the nature of the bond (ionic, covalent, or van der Waals) also is important. The character of the chemical bond is strongly influenced by the interfacial structure and chemistry on an atomic scale. Thus, in a study of composites it is important to characterize specific interfaces atomically and correlate the interface chemistry and structure to the macroscopic mechanical properties.

In this paper, a detailed examination of the interfaces of an Al/TiC composite is reported for the first time. The particles of TiC were precipitated exothermically *in situ* in Al melt, allowing interfacial contact between Al and TiC.

II. BACKGROUND

Many interfaces in composites such as those in Al/SiC,[1] Al/B$_4$C,[2] and Ti/SiC[3] can be categorized as multiphase interfaces because definite chemical reaction products are present at the interfaces. The wetting mechanism between the liquid metal and the ceramic particle is a chemical reaction between the matrix and the reinforcement producing additional phases. Such reaction products are often brittle in nature and detrimental to mechanical properties, especially room temperature ductility and fracture toughness. The presence of a reaction phase at the interface as well as contamination during processing prevent a direct low energy interface from being attained between the matrix and the dispersed phase.

A number of nonreactive metal-ceramic interfaces have been studied by high resolution transmission electron microscopy. Noteworthy are Nb/Al$_2$O$_3$,[4,5] Ag/CdO,[5] and Cu/Al$_2$O$_3$.[6] These composites were prepared by solid-state processes such as internal oxidation, epitaxial techniques, or diffusion bonding. The interfaces were free of impurities because of the processing technique. These studies have yielded results on interfacial structure and the nature of the bonding. Orientation relations between dispersed phase and matrix are seen similar to the case of solid-state precipitation caused by a change in solubility.

Interfaces free of contamination also may be produced by reactions in liquid metal by the XD *in situ* processing technique.[7] Semicoherent interfaces were ob-

served by Wang and Arsenault[8] between NiAl and *in situ* precipitated Al$_2$O$_3$ particles in *XD* NiAl/Al$_2$O$_3$/TiB$_2$ composites. In *XD* Al/TiC composites, both Al and TiC have fcc lattices and *Fm3m* symmetry. For a cube-on-cube orientation, they have a lattice mismatch [(a_{TiC} − a_{Al})/a_{TiC}] of 6.2%. (Here *a* is the lattice parameter; a_{Al} = 0.40496 nm and a_{TiC} = 0.43176 nm.) TiC has the B1 or NaCl structure with C atoms located at octahedral sites. Bramfitt[9] has shown from his study of solidification of δ-iron on substrates of different compounds that those that have smaller lattice mismatch are more effective in promoting nucleation. TiN and TiC, which have planar disregistry with respect to iron of 3.9% and 5.9%, respectively, are more efficient sites for heterogeneous nucleation than the other substrates examined. From similar arguments, TiC is expected to act as a heterogeneous nucleation site for solidification of Al, and, in fact, this has been demonstrated by Banerji and Reif.[10] TiC was precipitated *in situ*, and, hence, clean TiC surfaces acted as efficient nucleation sites. In another investigation, an epitaxial orientation relationship, (001)Al ∥ (001)TiC and [001]Al ∥ [001]TiC, was found by Cisse *et al.*[11]

From sessile drop tests, the contact angle between liquid Al and TiC was found to be less than 90°, showing excellent wetting.[12] In his investigation, Rhee reported that wettability of various particles by liquid Al is in the order AlN < TiB$_2$ < TiN < TiC and increases with increasing temperature. The good wettability of TiC by metallic Al was attributed to the metallic nature of TiC and the high chemical activity of Al. TiC is also partly ionic because of charge transfer from the 3*d* level of Ti to the 2*p* level of C.[13]

While TiC and Al are in equilibrium during *XD* processing, a chemical reaction between Al and TiC leading to the formation of Al$_3$Ti and Al$_4$C$_3$ takes place at temperatures below 1025 K.[14] The reaction is sufficiently slow at processing temperatures that no evidence for it is found after extrusion at 648 K.

Besides the chemical natures of the substrate compound and the metal, the crystallography of the substrate surface also plays a dominant role in wetting, as reported in an investigation of wetting of MgO single crystals (another NaCl structured compound) by liquid Pb, Sn, and Bi.[15] The degree of polarization, type of charge distribution, and atomic arrangements on the surfaces of MgO control the degree of wetting by the liquid metal. The same behavior is expected in the case of TiC. The TiC (111) and (100) surfaces have been studied using photoluminescence[16] and theoretical modeling.[17] In the TiC B1 structure, the (111) surfaces consist either entirely of Ti or of C atoms and are charged. In the Ti-ended (111) surfaces, each Ti atom has 3 C and 9 Ti nearest neighbors. It has been concluded from the photoemission spectrum that such a surface has a high

local density of states (LDOS) in the vicinity of the Fermi energy (E_F), as is also the case for the Ti(0001) surface.[16] A high local density of states near the Fermi energy results in the electrical conductivity of metals and their metallic nature. Thus, the Ti-terminated (111) TiC surface is expected to have electronic properties of a metal similar to the Ti(0001) surface, and its bonding with a metal across this interface is expected to have a highly metallic character.

At (100) surfaces in TiC, each Ti atom has 5 C and 8 Ti atoms as nearest neighbors as compared with bulk, where a Ti atom has 6 C and 12 Ti nearest neighbors. The (100) surfaces differ from (111) surfaces in that the former are made up of equal numbers of both atoms and are charge neutral. This arrangement can lead to a weaker interaction with Al. However, the presence of C vacancies changes the situation. In this case, a maximum is observed in LDOS near E_F.[18] This increases the reactivity of Ti centers on the (100) surface. Hence, it is probable that there is a strong electronic- or metallic-bonding mechanism with Al at a (100) TiC interface.

III. MATERIAL PREPARATION

Aluminum with 15 vol. % TiC of an average particle diameter 0.7 μm was produced by the two step *XD* (exothermic dispersion) process.[7,19] First, TiC was precipitated *in situ* in molten Al by the exothermic reaction of Ti and C. This step produced a high volume fraction "master alloy". In the second step, the *XD* master alloy was diluted with 99.99% pure aluminum and cast into a 75 mm diameter mold. This ingot was then extruded at 648 K with a 27:1 extrusion ratio. Most of the TiC particles produced are single crystals with surfaces free of impurities. Because of excess Ti in the first step, some Al$_3$Ti particles also were formed by a peritectic reaction, giving 0.5 vol. % of Al$_3$Ti particles in the final alloy.

The 2024 Al (Al + 3.5% Cu + 1.5% Mg) alloy dispersed with 15 vol. % of 0.3 μm particle size TiB$_2$ was cast in the same way and extruded at a 16:1 ratio. The composite was solution treated at 766 K for 2 h followed by water quenching. This was then naturally aged to the T4 condition (solution treated and aged at room temperature to a stable matrix microstructure).

Both composites were prepared by the Martin Marietta Corporation and delivered in the extruded condition. These were used for a study of interface structure and chemistry down to the atomic scale, and the results were correlated with the elastic modulus.

IV. EXPERIMENTAL PROCEDURES

Transmission electron microscopy samples were prepared by mechanical polishing to a thickness of 10–15 μm, followed by argon ion thinning using a

liquid nitrogen-cooled stage. The as-extruded composites were studied extensively by conventional transmission electron microscopy (CTEM) using a Hitachi H700-H TEM. High resolution transmission electron microscopy (HRTEM) of the interface was done on a Hitachi H-9000 TEM operating at 300 kV (spherical aberration = 0.95 mm, focal spread = 8 nm, and convergence = 0.5 mRad). To obtain lattice images it is necessary to tilt the sample so that a low index zone axis lies parallel to the beam direction. The orientation relationship between the Al matrix and a TiC particle usually is not simple. In the absence of a simple orientation relationship between the two phases it is not possible to have a perfectly aligned zone-axis on each side of their interface, a circumstance that limits quantitative interpretation of the micrographs. However, it was possible to tilt the goniometer stage so that one side had a low index zone axis parallel to the beam, whereas the other side had one set of low index planes parallel to the beam. This gave only one-dimensional fringes as the projection on the second side. It is also necessary that the interface be parallel to the beam. Only the cases in which an edge-on interface could be obtained by tilting were used for drawing any inference on structure.

Analytical microscopy was done on a Hitachi HF-2000 TEM equipped with a field emission gun operating at a voltage of 200 kV and an ultrathin window Link. A liquid nitrogen-cooled specimen holder was used to prevent contamination and damage. The probe size used for this work was about 3 nm.

Young's modulus of the XD Al/TiC composite was determined dynamically by measuring the resonant frequency of a longitudinal standing wave in a composite oscillator consisting of a quartz crystal and a matched sample of appropriate dimensions cemented together.[20] Knowing the resonant frequency of the quartz crystal (75 kHz) and the masses of the sample and the crystal, the resonant frequency f of the sample can be determined. The modulus E then was calculated from the folllowing equation:

$$E = 4l^2 \rho f^2 / n^2 \qquad (1)$$

where l is the length of the sample, n is an integer (1 for the first harmonic, this case), and ρ is the sample density.

V. RESULTS AND DISCUSSION

A. Microscopy

The TiC particle distribution obtained by the XD process followed by extrusion is fairly uniform. The particles are distributed in the matrix grain interiors as well as at grain boundaries. Figure 1 shows a grain of Al that is divided into subgrains. The particle labeled P is
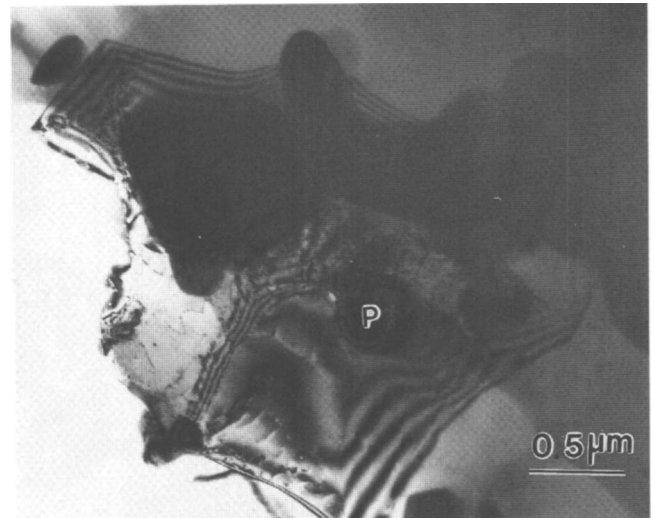

FIG. 1. TEM micrograph showing an Al grain with TiC particles located both inside the grain as well as at boundaries. The particle labeled P is inside the grain. The Al grain is divided into subgrains.

located inside the grain and has an edge-on interface with Al, as verified by dark-field imaging. Some grains have low angle boundaries inside them. Low angle boundaries probably formed during hot extrusion. The shapes of Al grains vary from fairly equiaxed to irregular when observed through a section perpendicular to the extrusion direction. The grain size varies between 1.5 and 3 μm transverse to the extrusion direction.

The TiC particles generally are polygonal in cross section and faceted. The size of most particles lies between 0.3 and 1.3 μm, with an average value of 0.7 μm. There are a few larger particles outside this range, up to 1.7 μm in size, but such particles were rarely seen. Some TiC particles appear to be bicrystals with low angle boundaries, as inferred from Figs. 2(a)–2(c). Figures 2(a) and 2(b) are bright- and dark-field micrographs of a twist boundary made up of a hexagonal network of dislocations. These dislocations are not believed to be from an interface with Al because they do not appear from an Al reflection at any orientation. Figure 2(c) represents a tilt boundary in TiC.

The single-crystal TiC particles also contain networks of dislocations, which probably cause the steps at the particle matrix interfaces. Figures 3(a)–3(e) show one such example of a network. Figure 3(a) shows a bright-field micrograph with two kinds of dislocations marked A and B. Figures 3(b)–3(e) show dark-field micrographs taken at different orientations under two beam conditions, namely, (022), (02$\bar{2}$), (311), and (1$\bar{1}$1). These dislocations have been analyzed using the $g \cdot b = 0$ criterion (g = reflection used and b = Burgers vector). Dislocations of type A disappear with reflections (311) and (022), which indicates that they are of screw character with a Burgers vector of 1/2[0$\bar{1}$1] or 1/2[01$\bar{1}$].

(a)
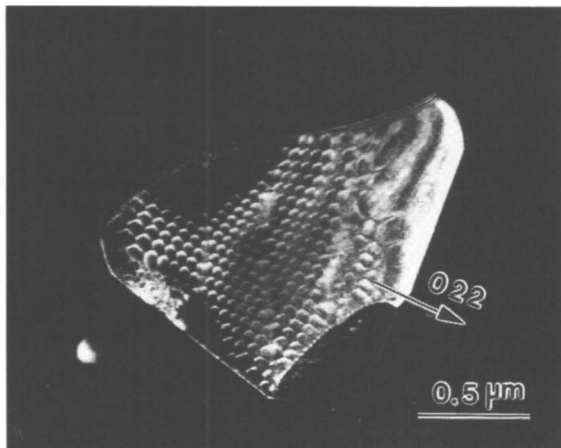
(b)
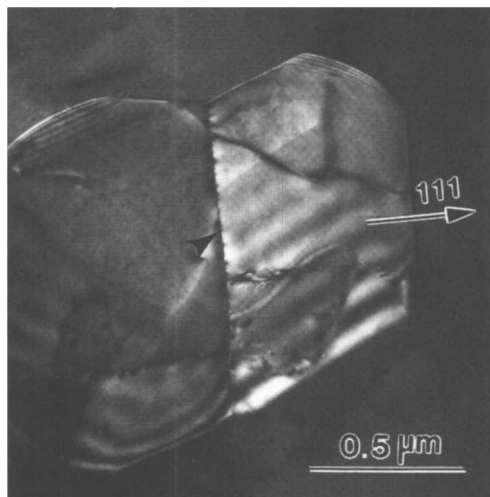
(c)

FIG. 2. TEM micrographs of low angle boundaries inside TiC: (a) bright- and (b) dark-field micrographs of a TiC particle containing a twist boundary made up of a hexagonal network of dislocations. (c) Dark-field micrograph of a tilt boundary inside a TiC particle.

Dislocations of type B appear to be of edge or mixed nature as the contrast does not disappear completely under any reflection. A thorough analysis of dislocations in other particles also showed Burgers vectors of type $1/2\langle 110\rangle$, as expected in face-centered cubic systems. A large number of particles contain three kinds of dislocations that form hexagonal networks.

The TiC particles probably grow by a ledge mechanism as suggested by the micrographs of Fig. 3(e) and Figs. 4(a) and 4(b), which are bright- and dark-field micrographs of particles in which the dislocations are rather random in distribution, and the interfaces have irregular steps. Atomic scale faceting can be seen at higher magnification, as discussed below. The dislocations in TiC are not likely to have formed during extrusion as the bulk TiC does not undergo slip at temperatures below 1073 K, which is above the melting point of Al.[21]

Observation by CTEM did not disclose any reaction product at the interfaces in the extruded condition. The interfaces can be compared to grain boundaries in metals and ceramics, which are of two kinds: those with misfit localization, called hereafter "special" orientation boundaries, and those that do not have any periodicity and do not show any misfit localization. Figure 5(a) shows a TiC particle located at an Al grain boundary. The interface is viewed almost edge-on. No strain contrast can be seen at this interface. However, a few interfaces indicate a certain degree of coherency. The interface in Fig. 5(b) contains an array of facets and periodically arranged dislocations along the interface. The approximate distance among the dislocations is 9 nm. This configuration is accompanied by strain contrast inside the Al matrix, proving that this situation is different from that in Fig. 5(a). Figures 5(c) and 5(d) also show strain localization at an interface, but in these examples the average distance between the positions of peak misfit strain is 22 and 36 nm, respectively. An examination of a number of particles with strain contrast showed that the average distance among peak misfit strains lies between 10 and 50 nm. Similar strain contrast has been observed at the semi-coherent interphase interfaces of directionally solidified eutectic NiO−ZrO$_2$ by Dravid *et al.*[22] The misfit strain contrast is believed to be caused by relaxation in the positions of atoms to accommodate the deviation from exact coincidence. Usually, TiC particles inside grains or those associated with low angle boundaries in Al show this tendency. Only parts of the particle may show misfit localization, as shown by viewing in various orientations. The strain contrast here is not perfectly periodic. This phenomenon has also been observed for the interphase interfaces in Pd/NiO internally oxidized composite and grain boundaries of Au by Merkle.[23] The deviation from periodicity has been attributed to misfit localization along incommensurate planes, which
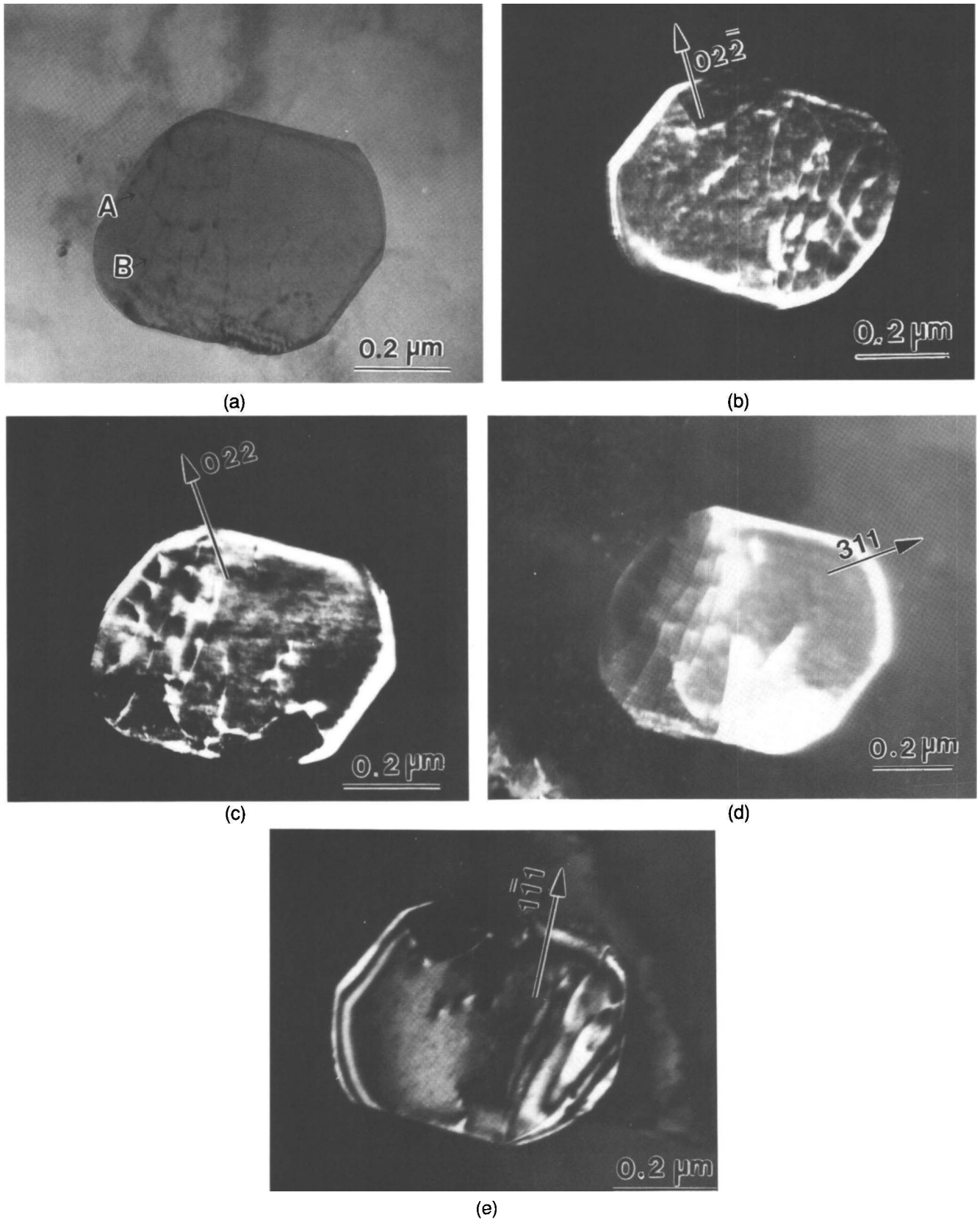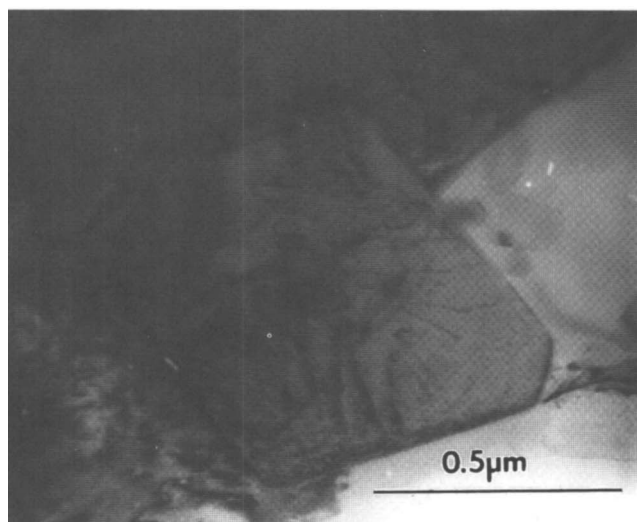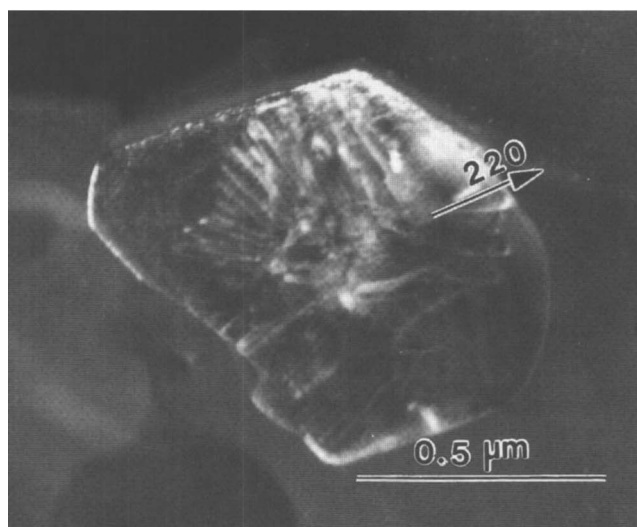
(a)

(b)

(c)

(d)

(e)

FIG. 3. TEM micrograph of a TiC particle showing dislocations. (a) A bright-field micrograph of a particle showing a dislocation network. (b)–(e) Dark-field micrographs of a faceted TiC particle imaged under different diffraction conditions. They show dislocations involved in the network, which produce a faceted morphology.

(a)

(b)

FIG. 4. TEM micrographs showing a TiC particle with a faceted surface created by dislocations seen in (a) bright field and (b) dark field [orientation is different from that of (a)].

is possible here as Al and TiC have different interplanar spacings. Additional information was obtained about Al/TiC interfaces from high resolution TEM images. These have clearly shown that interfaces are atomically abrupt, allowing direct contact between atoms of both phases. No reaction product is observed. Certain other interesting observations could be made. Figure 6 is a high resolution TEM micrograph of an interface between TiC and Al. The TiC is in an approximately [011] zone axis orientation. Al is not in a zone axis orientation. It is obvious that the interface plane of TiC is (11$\bar{1}$). This and similar observations show that there is a tendency of TiC to have densely packed planes at interfaces. Figures 7

through 9 were taken from different parts of a single TiC particle. Here TiC is oriented with the electron beam parallel to its [011] zone axis, and Al is tilted slightly away from its [011] zone axis. Figure 7 shows a curved part of the interface, which is faceted on an atomic scale with the facets parallel to the low index (11$\bar{1}$) and (200) planes of TiC. From a number of such observations, it is inferred that interfaces are parallel to low index and densely packed (111) or (100) planes in TiC. The {111} and {100} surfaces are the expected low energy surfaces in fcc crystals. Faceting at the interfaces along certain crystallographic directions suggests a tendency to lower interfacial energy.[22] However, as TiC has a partially ionic character,[13] the TiC{111}-vacuum surfaces are expected to be of a dipolar nature and are supposedly unstable as free surfaces.[24] But inside the metal the (111) interfaces with the matrix are stabilized by electronic interactions, as discussed earlier in this paper, and electronically bonded to Al.

Unlike the interface in Fig. 7, the interface in Fig. 8 is flat and parallel to the (11$\bar{1}$) TiC plane. From the optical diffraction pattern from the Al part of the image, it is apparent that the interface is parallel to a high index plane of Al. The lattices of Al and TiC are undistorted up to the interface. This is an asymmetric boundary as the lattice spacings of Al and TiC are different and also because of the orientation relationship between the Al and TiC grains. In asymmetric boundaries, the energy is lowered by having a densely packed or low index plane of at least one of the phases parallel to the interfacial plane.[25] Gao and Merkle[26] have observed densely packed planes occurring as interfacial planes in equilibrium and nonequilibrium boundaries giving better bonding and lower interfacial energy. Of course, densely packed planes at the interface will maximize the number of atoms interacting at the interface. It is postulated that having TiC {111} planes at interfaces aids in forming strong bonds of a metallic nature and lowering the interfacial energy.

Figure 9 shows what appears to be a stacking fault inside TiC close to the interface on the ($\bar{1}$11) planes. It is bound by the *X*'s. This defect causes a localized distortion in the TiC lattice close to the interface. Distortions in HRTEM images can also be expected because of changes in thickness, where the position of fringes can shift by half an atomic distance at half the extinction distance.[27] That does not appear to be the case here. In simulated images of TiC such transitions do not take place at the [011] zone axis with small changes in thickness at any of the defocus values. High symmetry zone axis images are not very sensitive to changes in thickness. A very sharp change in thickness inside TiC within 3 atomic spacings is unlikely. Thus, it is concluded that the image in Fig. 9 shows a genuine defect in the lattice. An edge dislocation (noted with
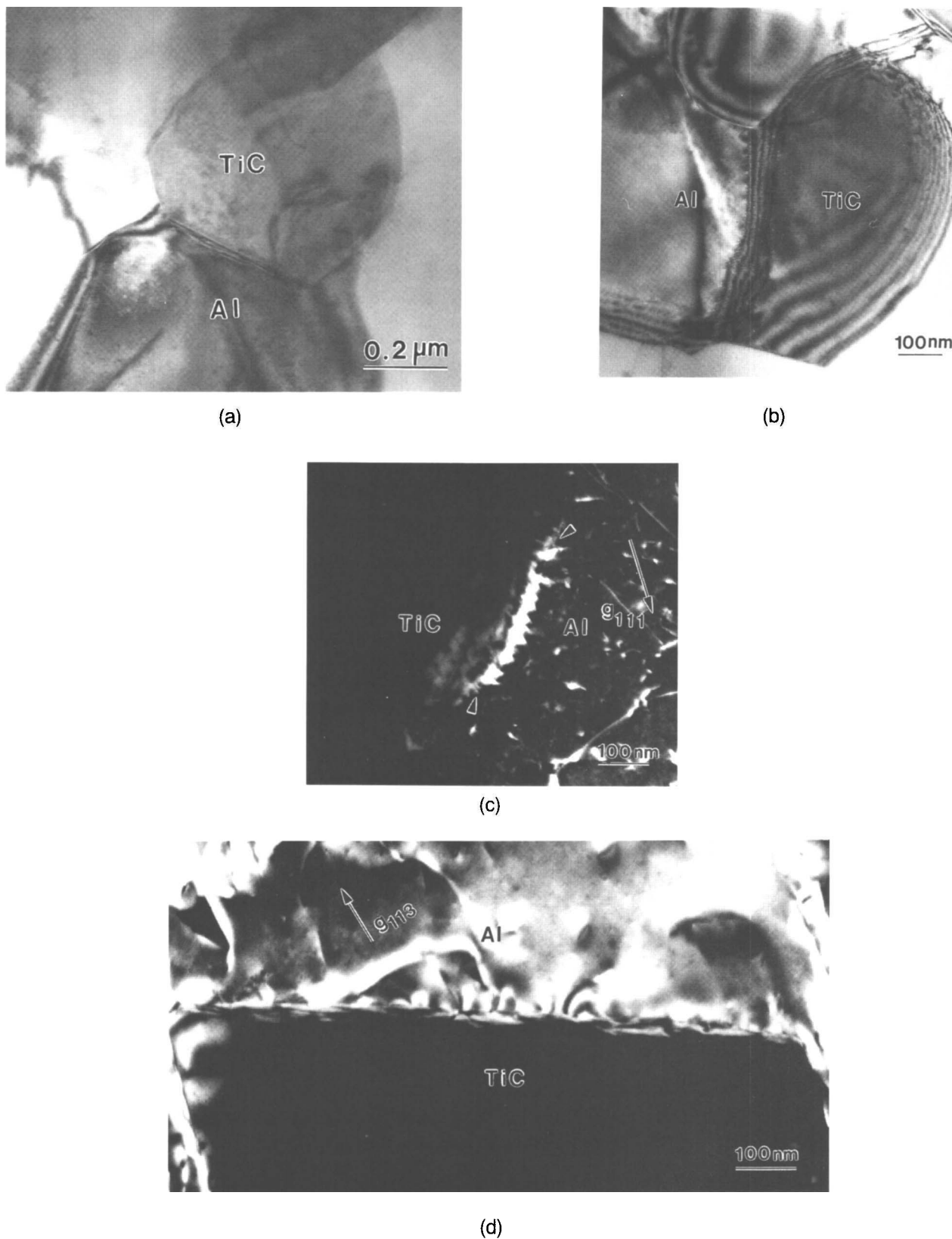
(a)

(b)

(c)

(d)

FIG. 5. TEM micrographs of different Al/TiC interfaces: (a) bright-field image of an incoherent boundary near edge-on orientation. The particle is situated at the Al grain boundary; (b) bright-field image of a semicoherent interface, where dislocations and fine-scale facets can be seen, (c) dark-field image of an interface showing misfit strain contrast (shown in between arrows), and (d) another dark-field image showing a particle with interface misfit localization.
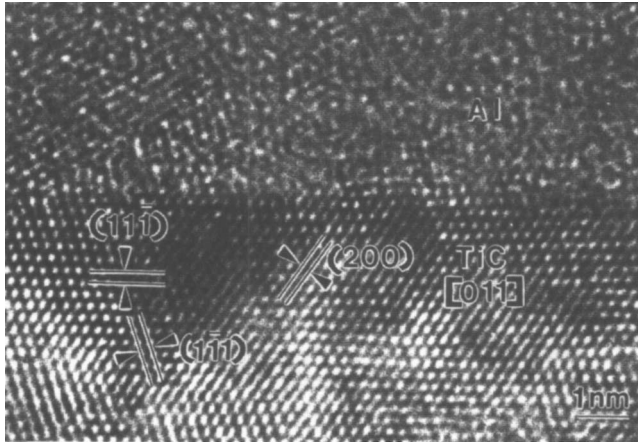
FIG. 6. A high resolution TEM micrograph of an almost flat interface. The TiC is close to [011] zone axis orientation, but Al is off from any low index orientation. The interface on the TiC side is parallel to (11$\bar{1}$).

an arrow) can also be seen inside the TiC. A carbon deficiency in TiC near the interface caused by defects can enhance the bonding between particle and matrix, as discussed above. Such defects near interfaces have been seen in other particles also.

Stoneham and Tasker[28,29] have shown through calculations that electrostatic image forces due to differences in dielectric constants between the metal and the oxide or carbide ceramic play a significant role in metal/ceramic bonding. The effect is strengthened if there are charged defects on the surface of the ceramic. Actually, the energy associated with the defect is lowered if it is close to an interface with a metal rather than a vacuum. Hence, a carbide such as TiC or an oxide that can lose its stoichiometry easily is wetted better by the metal. Nogi *et al.*[15] found from atom force microscopy that changes in atomic structure on the surface of a MgO crystal affect wetting behavior of metals strongly.

Clearly, no coherency strains were found inside Al at the interfaces in Figs. 7–9. Examples have been given of Al/TiC interfaces both with and without coherency strains (e.g., Fig. 5). While the processing route of this material makes it unlikely for all interfaces to have special relationships, a natural tendency to form low energy boundaries between Al and TiC is expected from the fact that TiC acts as a nucleant for Al grains during solidification, as already discussed,[10,11] and during recrystallization.[30] Also, the crystallographic and electronic nature of TiC surfaces should encourage
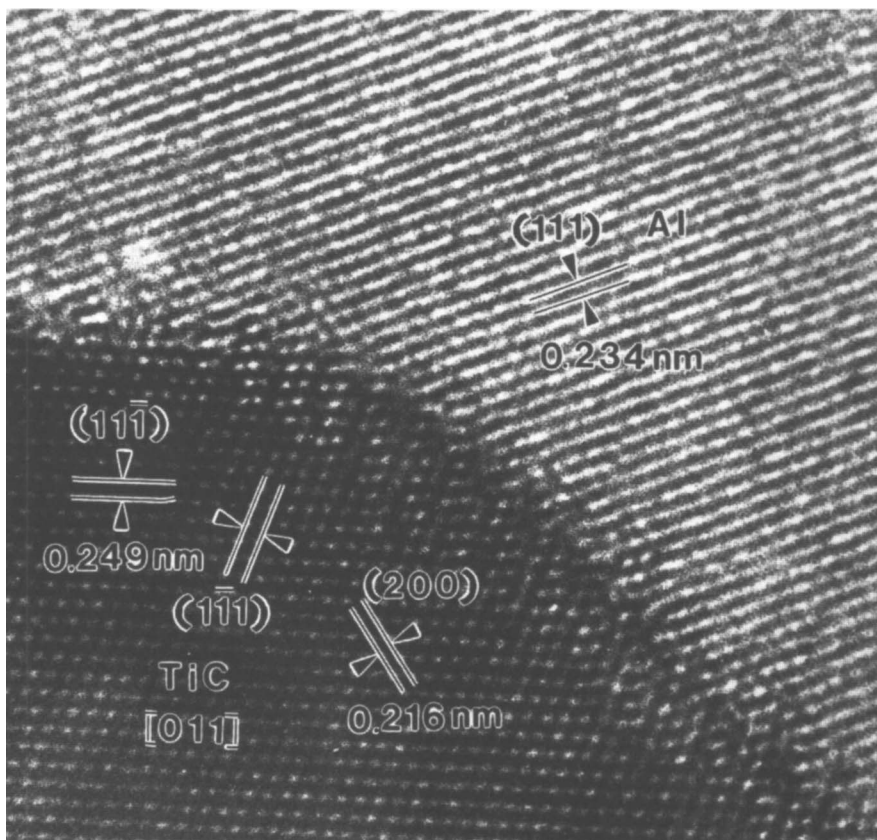

FIG. 7. A high resolution TEM micrograph of a curved interface, showing ledges parallel to (200) and (1$\bar{1}$1) planes of TiC. The image has been recorded with the beam parallel to the [011] zone axis of TiC.
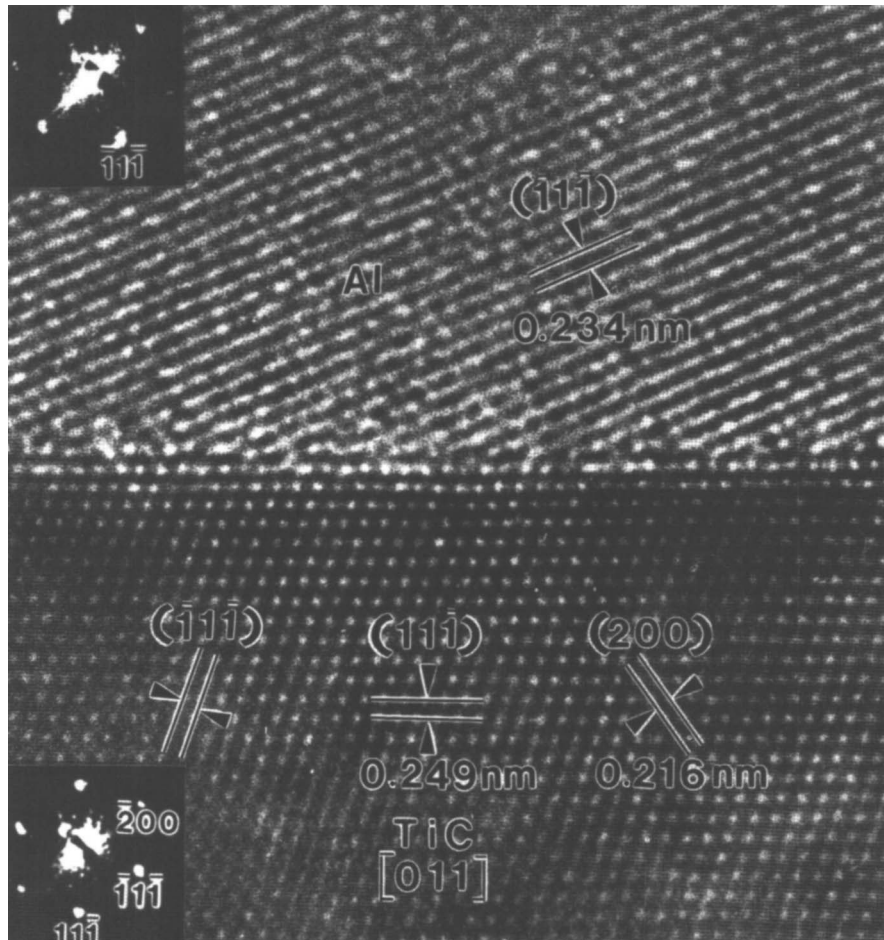
FIG. 8. A high resolution TEM micrograph of the flat part of an Al/TiC interface. The lattices of Al and TiC are undistorted up to the boundary. The optical diffraction patterns (011) from inside the lattices of Al and TiC are shown.

strong interaction between Al and TiC in the absence of any intermediate phase.

Composites of 2024 Al alloy-TiB$_2$ prepared by the *XD* process followed by extrusion also contain special boundaries. Figure 10 is an example of a semicoherent interface, as indicated by the strain contrast. Lattice imaging showed clean interfaces with direct contact between Al and TiB$_2$, but no structural information was obtained.

To find out if there is any segregation of the alloying elements at the interfaces in 2024 Al/TiB$_2$ composite, EDAX spectra were taken in Al close to and away from an interface. The analytical mode was used on the microscope with a probe size of about 3 nm. If there is segregation of magnesium near the interface, as is seen in the case of P/M 2124 Al/SiC,[31] a high intensity Mg peak is expected at, and close to, the interface with intensity decreasing inside the matrix. Figures 11(a) and 11(b) are spectra from a distance of approximately 2 nm (closest possible without picking up any x-rays from TiB$_2$) and 4 nm from the interface. The intensities of

the Mg and the Cu peaks do not change with distance from the interface. This indicates that there is no gradient in these elements from the interface to the bulk, at least as resolvable in the present experimental technique. Since there was no inert gas sputtering system inside the microscope, an O peak of the same intensity in both spectra was seen. One of the Ti peaks is close to that of an O peak, but still they can be easily distinguishable from one another. Figure 11(c) is a spectrum from deep inside the TiB$_2$ particle. There is no visible presence of oxygen as there is no Al, but there is a strong Ti peak.

B. Modulus measurements

Young's modulus of the composite is expected to increase with an increase in volume fraction of the ceramic reinforcement. Hashin and Shtrikman (H–S) used a variational technique based on linear elasticity theory to calculate the upper and lower bound values of the elastic constants for two phase materials.[32]

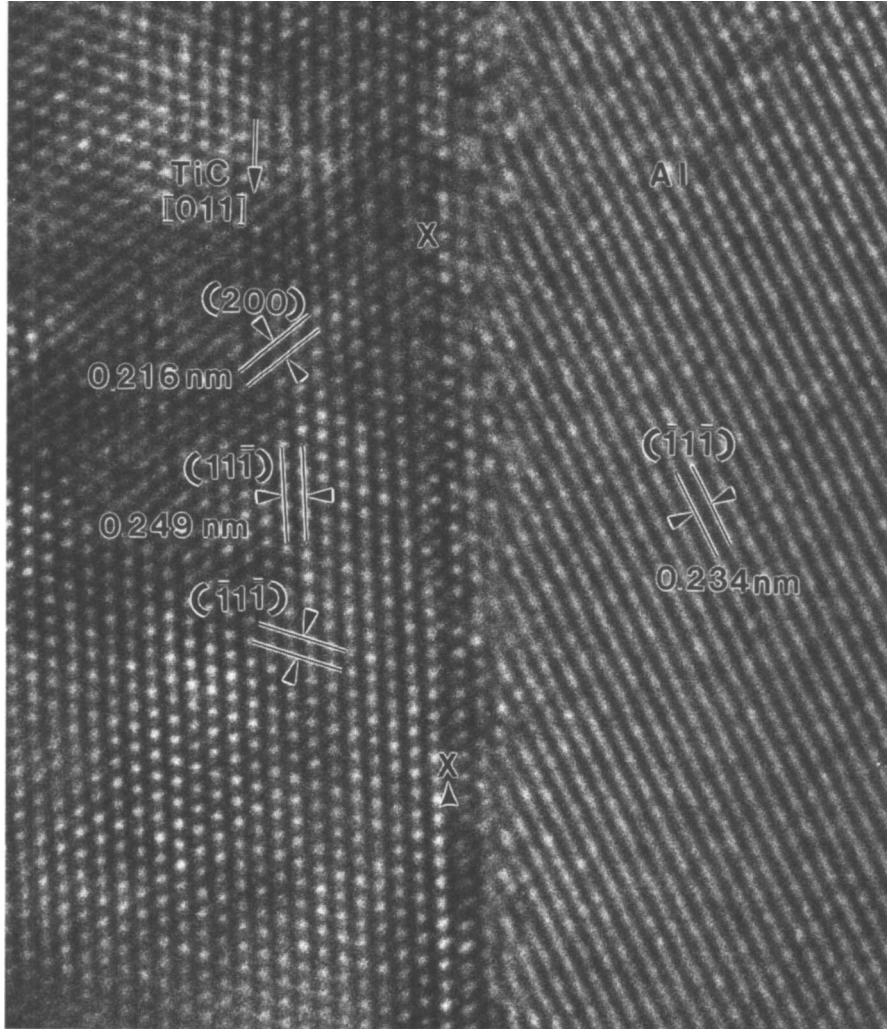The H–S relations assume elastic isotropy and a quasihomogeneous solid. Quasihomogeneity of a multi-

FIG. 9. A high resolution TEM micrograph of an Al/TiC interface in the as-extruded composite. First, 3 atomic layers inside TiC near the interface appear distorted, probably by a stacking fault between the *X*'s. Note the dislocation at the arrow.

phase solid is interpreted by assuming a reference cube, which is large compared to the size of the inhomogeneities, but is small compared to the whole body. The volume averages of the quantities like displacement, strain, stress, or phase volume fraction are the same for the whole body and the reference cube. The effective elastic modulus has been defined in terms of the strain energy stored in the solid when subjected to gross uniform stresses or strains, and upper and lower bounds are calculated using variational principles. Hashin and Shtrikman used isotropically fluctuating space functions like displacement, whose mean value was known, to find elastic strain energy.

The H–S relations predict the effective bulk and shear moduli, K^C and G^C, respectively, for the composite as:

$$K^C_{\text{lower}} = K_m + f/$$
$$\{[1/(K_p - K_m)] + [3(1 - f)/(3K_m + 4G_m)]\} \quad (2a)$$

$$K^C_{\text{upper}} = K_p + (1 - f)/$$
$$\{[1/(K_m - K_p)] + [3f/(3K_p + 4G_p)]\} \quad (2b)$$

$$G^C_{\text{lower}} = G_m + f/$$
$$\{[1/(G_p - G_m)] + 6(K_m + 2G_m)(1 - f)/$$
$$[5G_m(3K_m + 4G_m)]\} \quad (2c)$$

$$G^C_{\text{upper}} = G_p + (1 - f)/$$
$$\{[1/(G_m - G_p)] + 6(K_p + 2G_p)f/$$
$$[5G_p(3K_p + 4G_p)]\}, \quad (2d)$$

where f is the volume fraction of the particles, K is the bulk modulus, G is the shear modulus, and the subscripts m and p refer to matrix and particles, respectively. Equation (2a), the lower limit of the bulk modulus, is obtained assuming that the phase p is distributed in the
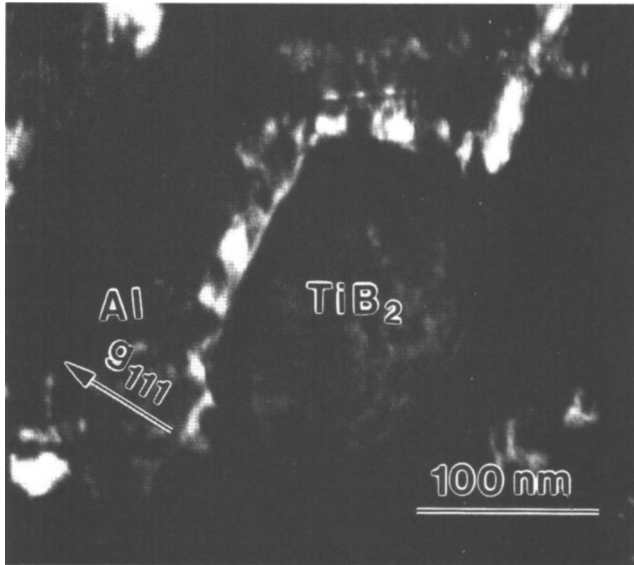
FIG. 10. Dark-field TEM micrograph of a 2024-Al alloy/TiB$_2$ interface showing interface misfit localization.

matrix m, while Eq. (2b) is derived for the situation in which the phase m is the dispersed phase inside the matrix p. The same criteria are used to derive the lower and upper limits of shear modulus in Eqs. (2c) and (2d). The lower and upper bound values of Young's modulus E can be estimated from the relationship:

$$E = 9KG/(3K + G) \qquad (2e)$$

A chemically bonded interface will give an E value in the range estimated from these equations, whereas a mechanically bonded interface will fail to make even the lower bound value.

The modulus determined for the 0.7 μm particle size composite is plotted in Fig. 12 with the lower and upper bound curves as predicted by the H–S equations. The experimental modulus value for the Al/TiC composite is 93.8 ($\pm$1.5) GPa, which is close to the upper Hashin–Shtrikman limit. Similarly, *XD* composite 2124 Al–15 vol. % TiB$_2$ showed a modulus of 94 GPa, which is also close to the upper H–S limit.[33] The fact that the modulus of both *XD* composites is close to the upper H–S limit indicates that *XD* processing leads to a complete chemical interfacial bonding and the attendant load transfer.

VI. FINAL DISCUSSION

The composites in the present investigation were hot extruded at 648 K, which obviously changed the interface structures between Al and TiC existing in the as-cast stage. Partial recrystallization which took place during high temperature deformation is believed to have resulted in the formation of special orientation boundaries between Al and TiC. Al/TiC interfaces appear to have varying degrees of coherency, and misfit dislocations accommodate deviations from coincidence. Though it is not known how far these are from thermodynamic equilibrium, it is believed that these boundaries form to lower the interfacial energy. Obviously, the electronic interactions between Al and TiC vary with orientation. Maximization of the electronic interaction is one driving force for the formation of special boundaries. Relaxation occurs inside Al to lower the strain energy. The electronic nature of Ti-ended TiC {111} surfaces, which is similar to that of the Ti metal, is thought to lead to bonding of a metallic nature.

Certain other conclusions emerge from the observations of the present investigation. As TiC particles have their close-packed or low-index planes ({111} and {100}) parallel to the interface, it appears that the interfacial energy can be lowered in a way similar to that in asymmetric grain boundaries in metals and ceramics.[25] This and the presence of charged defects close to the interfaces inside TiC are thought to help give strong interaction with Al. Interfaces in *XD* Al/TiB$_2$ composites are free of segregants and many show semicoherency. However, as TiC has a modulus much higher than that of Al, relaxations take place essentially in Al at or close to the interface. Geometrical considerations are, however, not enough to determine the energy of metal-ceramic interfaces; the detailed electronic structure of interfaces is also needed.[34] In the case of Al/TiC interfaces, the metallic character of bonding is expected to be a maximum for the TiC {111} interface, as discussed.

The modulus of the Al/TiC composite is in the high range of the Hashin–Shtrikman prediction, showing that chemical binding between Al and TiC has occurred along with load transfer between the two phases. The interfaces are ductile and do not show cracking even after 75% reduction in thickness by cold rolling.[30] The Al/TiC composite has shown 20% elongation to failure in tension even at 15 vol. % reinforcement.[14] This is further evidence for a bond with a high metallic component.

VII. CONCLUSIONS

(1) TiC particles precipitated in the *XD* process are highly faceted and contain dislocations with a Burgers vector of 1/2⟨110⟩ as expected in fcc lattices. The TiC surfaces in *XD* Al/TiC composite are parallel to low index {111} and {100} planes. These are thought to give strong bonds with Al of a highly metallic character. The composite is very ductile at room temperature.

(2) The interfaces obtained in *in situ XD* processing of Al/TiC are abrupt, and no impurities were detected. The particles have surfaces that are unoxidized, active, and free of contaminants because they are precipitated *in situ*.
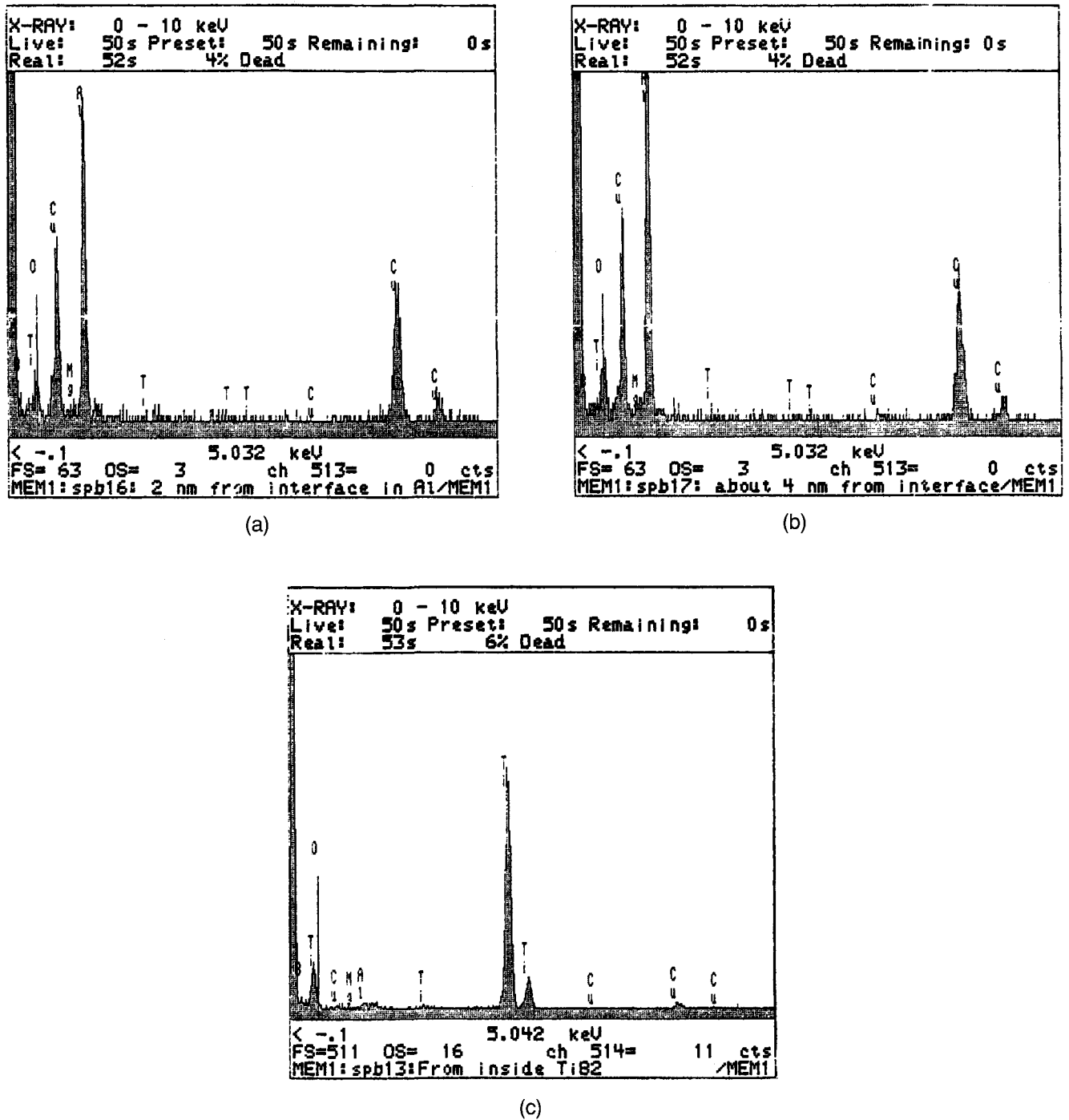
FIG. 11. EDAX spectra from an *XD* 2024-Al/TiB₂ composite: inside Al (a) 2 nm and (b) 4 nm from the interface, and (c) inside TiB₂.

(3) Special orientation boundaries form between Al and TiC with some degree of local coherency, if the particles are relatively small compared with the Al grains and lie inside the grains.

(4) Many interfaces in *XD* 2024 Al/TiB₂ also exhibit periodic strain contrast. No segregation of alloying elements could be found, and direct contact exists on an atomic scale.

(5) *XD* Al/TiC and 2024 Al/TiB₂ composites have shown Young's modulus values of 93.8 and 94.0 GPa, respectively, which are well within Hashin–Shtrikman limits in keeping with the strong interfacial bonding.
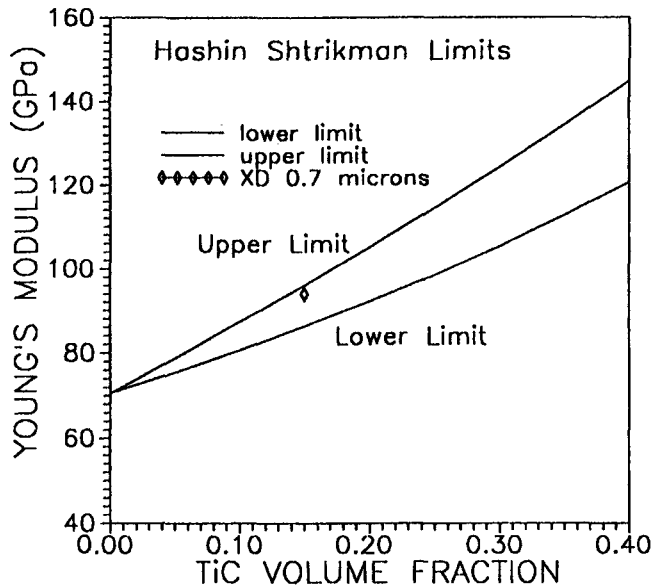
ACKNOWLEDGMENTS

FIG. 12. Variation of Young's modulus with volume fraction of TiC, according to Hashin–Shtrikman's model.[32] The data point shows the modulus value of the *XD* Al/TiC composite.

REFERENCES

1. S. Y. Oh, J. A. Cornie, and K. C. Russell, Metall. Trans. **20A**, 533 (1989).
2. J. P. Lucas, N. Y. C. Yang, and J. J. Stephens, in *Structure and Properties of Interfaces in Materials,* edited by W. A. T. Clark, U. Dahmen, and C. L. Briant (Mater. Res. Soc. Symp. Proc. **238**, Pittsburgh, PA, 1992), p. 877.
3. C. Jones, C. J. Kiely, and S. S. Wang, J. Mater. Res. **4**, 327 (1989).
4. W. Mader and M. Rühle, Acta Metall. **37**, 853 (1989).
5. W. Mader, Z. Metallk. **80**, 139 (1989).
6. F. Ernst, P. Pirouz, and A. H. Heuer, Philos. Mag. A **63**, 259 (1991).
7. A. R. C. Westwood, Metall. Trans. **19A**, 749 (1988).
8. L. Wang and R. J. Arsenault, Metall. Trans. **22A**, 3013 (1991).
9. B. L. Bramfitt, Metall. Trans. **1**, 1987 (1970).
10. A. Banerji and W. Reif, Metall. Trans. **17A**, 2127 (1986).
11. J. Cisse, G. F. Bolling, and H. W. Keer, J. Cryst. Growth **13/14**, 777 (1972).
12. S. K. Rhee, J. Am. Ceram. Soc. **53**, 386 (1970).
13. L. Ramqvist, J. Phys. Chem. Solids **30**, 1835 (1969).
14. R. Mitra, J. R. Weertman, and M. E. Fine, J. Mater. Res. **8**, 2370 (1993).
15. K. Nogi, M. Tsujimoto, K. Ogino, and N. Iwamoto, Acta Metall. Mater. **40**, 1045 (1992).
16. A. M. Bradshaw, J. F. Van der Veen, F. J. Himpsel, and D. E. Eastman, Solid State Commun. **37**, 37 (1980).
17. A. Fujimori, F. Minami, and N. Tsuda, Surf. Sci. **121**, 199 (1982).
18. A. L. Ivanovsky and V. A. Gubanov, in *Atomic Scale Calculations of Structure in Materials,* edited by M. S. Daw and M. A. Schluter (Mater. Res. Soc. Symp. Proc. **193**, Pittsburgh, PA, 1990), p. 161.
19. R. M. Aikin, Jr., Martin Marietta Laboratory, Baltimore, MD, private communications.
20. M. E. Fine, in ASM STP **129**, 1 (1952).
21. A. P. Katz, H. A. Lipsitt, T. Mah, and M. G. Mendiratta, J. Mater. Sci. **18**, 1983 (1983).
22. V. P. Dravid, C. E. Lyman, M. R. Notis, and A. Revcolevschi, Ultramicrosc. **29**, 60 (1989).
23. K. L. Merkle, in Proc. XIIth Int. Cong. Elec. Micro. (EMSA, San Francisco, CA, 1990), p. 332.
24. P. W. Tasker, J. Phys. C **12**, 4977 (1979).
25. D. Wolf, in *Ceramic Microstructures '86: Role of Interfaces,* edited by J. A. Pask and A. G. Evans (Materials Science Research, Plenum Press, New York, 1986), Vol. 21, p. 177.
26. Y. Gao and K. L. Merkle, in *Structure and Properties of Interfaces in Materials,* edited by W. A. T. Clark, U. Dahmen, and C. L. Briant (Mater. Res. Soc. Symp. Proc. **238**, Pittsburgh, PA, 1992), p. 775.
27. P. G. Self, R. W. Glaisher, and A. E. C. Spargo, Ultramicrosc. **18**, 49 (1985).
28. A. M. Stoneham and P. W. Tasker, J. Phys. C **18**, L543 (1985).
29. A. M. Stoneham and P. W. Tasker, in *Ceramic Microstructures '86: Role of Interfaces,* edited by J. A. Pask and A. G. Evans (Materials Science Research, Plenum Press, New York, 1986), Vol. 21, p. 155.
30. R. Mitra, W. A. Chiou, J. R. Weertman, M. E. Fine, and W. A. Chiou, in *Structure and Properties of Interfaces in Materials,* edited by W. A. T. Clark, U. Dahmen, and C. L. Briant (Mater. Res. Soc. Symp. Proc. **238**, Pittsburgh, PA, 1992), p. 871.
31. S. R. Nutt, in *Interfaces in Metal Matrix Composites,* edited by A. K. Dhingra and S. G. Fishman (TMS, Warrendale, PA, 1986), p. 157.
32. Z. Hashin and S. Shtrikman, J. Mech. Phys. Solids **11**, 127 (1963).
33. R. M. Aikin, Jr., Martin Marietta Laboratories, Report MML TR 63c, p. 118, 103, 108 (1990).
34. K. McCafferty, A. Soper, J. Shirokoff, and U. Erb, in *Structure and Properties of Interfaces in Materials,* edited by W. A. T. Clark, U. Dahmen, and C. L. Briant (Mater. Res. Soc. Symp. Proc. **238**, Pittsburgh, PA, 1992), p. 47.

2392

J. Mater. Res., Vol. 8, No. 9, Sep 1993